Wounding-induced changes in cellular pressure and localized auxin signalling spatially coordinate restorative divisions in roots

Lukas Hoermayer[a], Juan Carlos Montesinos[a], Petra Marhava[a,1], Eva Benková[a], Saiko Yoshida[a,2], and Jiří Friml[a,3]

[a]Institute of Science and Technology Austria, 3400 Klosterneuburg, Austria

Edited by Natasha V. Raikhel, Center for Plant Cell Biology, Riverside, CA, and approved April 27, 2020 (received for review February 21, 2020)

Wound healing in plant tissues, consisting of rigid cell wall-encapsulated cells, represents a considerable challenge and occurs through largely unknown mechanisms distinct from those in animals. Owing to their inability to migrate, plant cells rely on targeted cell division and expansion to regenerate wounds. Strict coordination of these wound-induced responses is essential to ensure efficient, spatially restricted wound healing. Single-cell tracking by live imaging allowed us to gain mechanistic insight into the wound perception and coordination of wound responses after laser-based wounding in *Arabidopsis* root. We revealed a crucial contribution of the collapse of damaged cells in wound perception and detected an auxin increase specific to cells immediately adjacent to the wound. This localized auxin increase balances wound-induced cell expansion and restorative division rates in a dose-dependent manner, leading to tumorous overproliferation when the canonical TIR1 auxin signaling is disrupted. Auxin and wound-induced turgor pressure changes together also spatially define the activation of key components of regeneration, such as the transcription regulator ERF115. Our observations suggest that the wound signaling involves the sensing of collapse of damaged cells and a local auxin signaling activation to coordinate the downstream transcriptional responses in the immediate wound vicinity.

regeneration | auxin | ERF115 | cell expansion | cell division

Plant cells are encapsulated by their rigid cell walls; hence, tissue regeneration in plants relies mainly on oriented cell divisions, directional cell elongation, and acquisition of new cell fates (1–4). We recently showed that ablation of small groups of cells in the root meristem can be used to study wounding responses and regeneration in vivo and on a single-cell level (5). These studies revealed that wounding triggers restorative cell divisions predominately in cells at the inner adjacent side of the eliminated cells. The accelerated divisions deposit new cell walls parallel to the wound area (usually in a periclinal orientation), and the newly generated daughter cells subsequently acquire the cell fate of the removed cells as they fill the wound. This process depends on the reactivation of stem cell components and division plane switch in these cells. Other recent studies using the single-cell ablation method investigated early wound responses in the root implicating calcium signaling, immune peptide activation, and jasmonate and ethylene signaling (6–8).

A key component of the wound response is the transcription factor ETHYLEN-RESPONSIVE 115 (ERF115), which is usually not expressed in the root meristem but whose expression is activated after wounding in close vicinity to the damaged tissue. ERF115 heterodimeric binding to different transcription factors induces downstream transcriptional reprograming, leading to dedifferentiation and proliferation (9, 10). Activation of ERF115 expression has been linked in different contexts to multiple signals, including brassinosteroids, jasmonic acid, auxin, and reactive oxygen species (6, 9, 11, 12). Although many of these upstream regulations have been implied, what defines the strict ERF115 spatial and temporal expression pattern remains elusive.

Auxin, a classical phytohormone, has a key role in many aspects of plant growth and development, and also has been proposed to be important in tissue and organ restoration during regeneration as it accumulates after amputation of the root tip above the wound and crucially contributes to the regeneration process (13, 14). Also during undisturbed development, auxin is involved in orienting cell division planes, in cell fate (re)specification, and in the maintenance of the root stem cell niche (15–17), all processes essential for tissue regeneration. Despite these indications, a specific role for auxin in wound healing and local tissue restoration has not been shown.

Here we show a local increase of auxin signaling specifically in wound-adjacent cells later undergoing restorative divisions. We identify a dual mode of action for auxin in wound-responsive cell division and expansion rates. Auxin, via its canonical, nuclear signaling, regulates cell division and ERF115 expression, both

Significance

Plants are sessile organisms that cannot evade wounding or pathogen attack, and their cells are encapsulated within cell walls, making it impossible to use cell migration for wound healing like animals. Thus, regeneration in plants largely relies on the coordination of targeted cell expansion and oriented cell division. Here we show in the root that the major growth hormone auxin is specifically activated in wound-adjacent cells, regulating cell expansion, cell division rates, and regeneration-involved transcription factor ERF115. These wound responses depend on cell collapse of the eliminated cells presumably perceived by the cell damage-induced changes in cellular pressure. This largely broadens our understanding of how wound responses are coordinated on a cellular level to mediate wound healing and prevent overproliferation.

Author contributions: L.H., J.C.M., P.M., S.Y., and J.F. designed research; L.H., P.M., and S.Y. performed research; J.F. contributed new reagents/analytic tools; L.H., P.M., and S.Y. analyzed data; L.H., J.C.M, and J.F. wrote the paper; and P.M., E.B., and S.Y edited versions of the paper.

The authors declare no competing interest.

This article is a PNAS Direct Submission.

Data deposition: Raw data in the form of microscopy images and compiled videos can be accessed at https://www.ebi.ac.uk/biostudies/BioImages/studies/S-BIAD23 under accession no. S-BIAD23.

[1]Present address: Department of Plant Molecular Biology, University of Lausanne, CH-1015 Lausanne, Switzerland.

[2]Present address: Department of Comparative Development and Genetics, Max Planck Institute for Plant Breeding Research, 50829 Cologne, Germany.

[3]To whom correspondence may be addressed. Email: jiri.friml@ist.ac.at.

This article contains supporting information online at https://www.pnas.org/lookup/suppl/doi:10.1073/pnas.2003346117/-/DCSupplemental.

First published June 15, 2020.

promoting and inhibiting wound responses in a dose-dependent manner. Finally, we show that ERF115 expression and wound-responsive cell division are linked spatially and temporary through the perception of damaged cell collapse, indicating a crucial role of turgor pressure and cell wall integrity perception in wound signaling.

Results

Local Auxin Accumulation in Cells Undergoing Restorative Division. To observe potential changes in auxin signaling after single-cell ablation, we used an auxin signaling marker, R2D2, which consists of an auxin-degradable RPS5::DII-Venus component and the stable RPS5::mDII-Tdtomato, allowing detection of increased auxin signaling (18). We used vertical growth confocal imaging coupled with live tracking (19, 20) to follow cells during regeneration over a prolonged period (16 to 32 h). We observed a down-regulation of DII-Venus indicative of auxin signaling increase in wound-adjacent cells approximately 3 h before the first division (Fig. 1 and Movie S1). These changes in DII were absent from neighboring cells not adjacent to the wound in the same roots. Notably, after the first division, daughter cells that were still adjacent to the wound retained the high auxin signaling activity, while the nonadjacent daughter cells quickly regained normal auxin signaling levels (Fig. 1 *A* and *C*). These dynamics were not due to any possible bleaching effects of the ablation or propidium iodide staining (*SI Appendix*, Fig. S1 *A–E* and Movies S2 and S3), and at least ∼50% of all wound-adjacent cortex and ∼20% of all wound-adjacent endodermis cells exhibited this down-regulation of DII-Venus (*SI Appendix*, Fig. S1*G*), altogether suggesting increased auxin signaling in cells activated by wounding.

To elucidate the source of this increased auxin signaling in the wound-adjacent cells, we performed long-term imaging of roots treated with the auxin biosynthesis inhibitors kynurenine and yucasin, as well as with the polar auxin transport inhibitor naphthylphthalamic acid (NPA) (21–23). Notwithstanding the overall auxin accumulation throughout the root tip after NPA treatment, we still observed consistent DII signal down-regulation specifically in the wound-adjacent cells compared with their direct neighbors (*SI Appendix*, Fig. S1*F* and Movie S4). A wounding-induced local increase in auxin signaling also occurred after inhibition of auxin biosynthesis (*SI Appendix*, Fig. S1*H* and Movie S5). Even though some role of these processes cannot be completely ruled out, these pharmacologic manipulations suggest that auxin biosynthesis or polar transport are not major contributors to the local increase in auxin signaling during regeneration. Other, as-yet unidentified auxin homeostasis processes, such as release of free auxin from conjugates, may play a role.

In summary, our findings show a local increase of auxin signaling in wound-adjacent cells, specifically those that contribute to the regeneration process by later restorative divisions and expansion. The underlying mechanism for this elevated auxin signaling remains elusive but appears to be independent of both onsite auxin biosynthesis and polar auxin transport.

Dual Auxin Effect on Regeneration Efficiency. The local increase in auxin signaling after wounding implies a role for auxin in restorative patterning. Auxin might accelerate the cell cycle progression and determine the cell division plane or the stem cell fate acquisition, the cell expansion toward the wound, or a combination of these effects. As reported previously (5), the

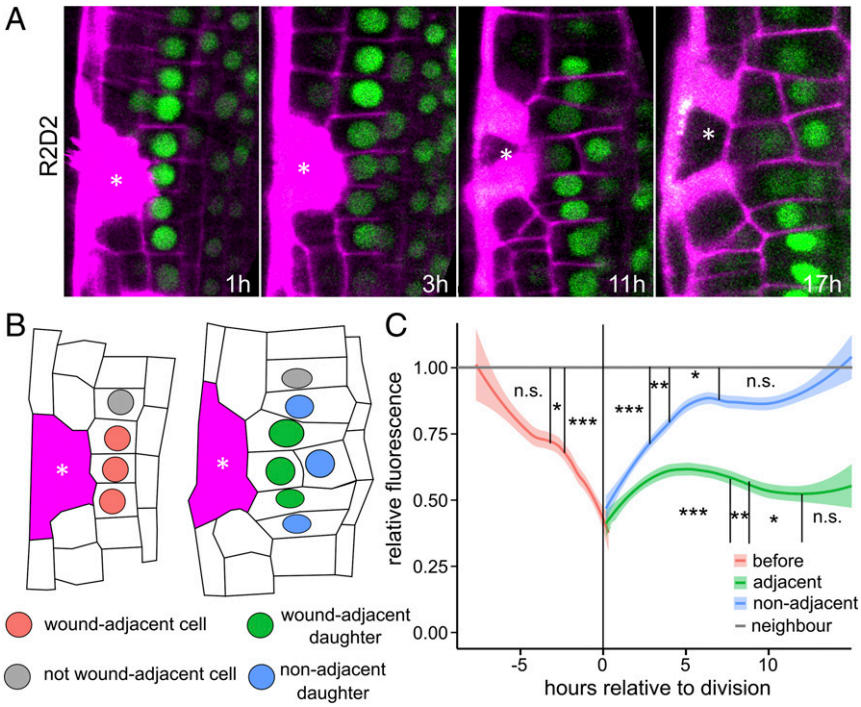

Fig. 1. Auxin signaling in wound-adjacent cells. (*A* and *B*) Wound-adjacent cells exhibit increased auxin signaling compared with neighboring cells. (*A*) DII-Venus (green) expression (of R2D2-negative auxin marker line) in cells next/adjacent to ablated cells (marked with asterisk) at 1, 3, 11, and 17 h after cell ablation. A lower DII-Venus signal indicates higher auxin signaling. Cell walls and dead cells are stained with PI (pink). (*B*) Schematic representation of wound-adjacent cells at different stages of regeneration. Ablated cell is in pink with an asterisk. (*C*) Quantification of DII-Venus fluorescence signal over time from wound-adjacent cells before cell division (red) or after cell division (wound-adjacent in green; non–wound-adjacent in blue). Data are represented as DII-Venus fluorescence in observed cells relative to neighboring, nonadjacent cells. Time "0 h" represents the time of restorative cell division. Thick lines represent the smoothed mean, and the lighter background represents smoothed SE from $n = 18$ cells each. Statistical significance was computed using a one-sample Wilcoxon test.

cortex and endodermis exhibit different rates of restorative, periclinal cell divisions after 12 h; endodermis cells divide rapidly, while division of cortex cells is usually slower. However, after sufficient time (>32 h), all ablated cells are replaced by restorative divisions of wound-adjacent cells.

To test for an auxin effect in wound regeneration, we applied synthetic auxin (1-napthylacetic acid [NAA]) 1 h before the ablation, imaged the wounded roots 12 h after ablation, and determined how many ablation sites triggered periclinal cell divisions in the inner adjacent cell types. These experiments revealed that NAA application increased the division rates at concentrations up to 1 μM (Fig. 2*A* and *SI Appendix*, Fig. S2*A*), particularly in cortex cells, which usually have a relatively low regeneration rate in the first 12 h. On the other hand, the already fast regeneration rate of the endodermis cells (~75%) was not much further increased by auxin (*SI Appendix*, Fig. S2*A*). To examine the effects of decreased auxin levels, we treated roots with 10 μM kynurenine and observed that roots with lower auxin levels exhibited decreased restorative division rates in all cell types, again indicating a positive auxin effect on restorative cell divisions (*SI Appendix*, Fig. S2*C*).

Nonetheless, at higher concentrations, NAA caused a decrease in division rates, with 1 μM NAA apparently representing a breaking point, where two populations of auxin-treated roots were observed: roots with fast and efficient regeneration similar to plants treated with 250 to 500 nM and roots with strongly inhibited regeneration. The inhibitory auxin effect became more pronounced at 2 μM NAA, and at 5 to 10 μM NAA, regeneration no longer occurred (Fig. 2*A* and *SI Appendix*, Fig. S2*A*). This concentration-dependent auxin effect on restorative division rates suggests a dual, both positive and negative, mode of action for auxin during tissue regeneration.

TIR1 Auxin Signaling-Mediated, Wound-Induced Cell Proliferation. To investigate the signaling mechanism underlying this auxin effect, we tested NAA application on the *tir1-1 afb2-1 afb3-3* (*tir triple*) mutant, which is defective in auxin receptors (24, 25). Untreated *tir triple* mutant showed a regeneration capacity not much different from that of the wild type (WT) (Fig. 2*B* and *SI Appendix*, Fig. S2*B*). However, in the *tir triple* mutant, treatment with 1 μM NAA, which in WT normally inhibited divisions, increased the restorative division rate of endodermis and cortex cells to almost maximum (Fig. 2*B* and *SI Appendix*, Fig. S2*B*); we even observed repeated divisions within 12 h (*SI Appendix*, Fig. S2*H*). This suggests that the dual-phase effect of auxin can be differentiated into an activating effect and an inhibitory effect on restorative divisions, with at least the latter effect depending on the activity of the TIR1 auxin receptors.

Besides its overall effect on the rate of restorative cell divisions, auxin also influenced the direct response of each involved cell toward wounding. Usually, wound sizes one to two cells are filled by one to three adjacent cells at the inner side of the wound, which initiate periclinal divisions (5); however, auxin treatment increased the area of activated cells to nearly all wound-adjacent cells. On some occasions, four or more cells responded to the wound by inducing restorative divisions (Fig. 2*C* and *SI Appendix*, Fig. S2 *D* and *E*). Auxin also triggered ectopic periclinal cell divisions at the outer wound side or in adjacent upper and lower cells. Usually, these cells undergo normal anticlinal divisions and do not contribute greatly to the wound healing (5) (Fig. 2*D* and *SI Appendix*, S2 *F* and *G*). This auxin effect on activating more adjacent cells and at all sides also occurred in the *tir triple* mutant and thus is likely a component of the activating auxin effect that is less dependent on TIR1/AFB-mediated auxin perception.

These effects of auxin on the increase in restorative division rate, the spreading of wound responses to all adjacent cells, and the ectopic division plane switch from anticlinal to periclinal were regularly manifested in an overproliferation of the whole wounded area. Roots treated with 1 μM NAA sometimes contained wound-responsive cells that did not stop the periclinal cell divisions and continuously divided and expanded to overfill the induced wounds with new daughter cells. This caused a strong swelling of the root meristem (Fig. 2*G*), which occurred in ~20 to 50% of WT plants. However, in the *tir triple* mutant, most ablation sites (60 to 70%) triggered this strong overproliferation phenotype, likely because of a reduction in the TIR1 signaling-mediated inhibitory auxin effect (Fig. 2 *E* and *F* and *SI Appendix*, Fig. S2*I*).

To further test the involvement of TIR1 in this regulation, we used the synthetic CCV-TIR1–convex IAA (CVX-IAA) pair, in which a modified auxin ligand, CVX-IAA, can bind only to a mutated form of TIR1 receptor, CCV-TIR1, but not to WT-TIR1 (26). CVX-IAA triggered swelling only in the *CCV-TIR1* plant, but not in the WT plants (*SI Appendix*, Fig. S2*J*).

This causally links the auxin effect on wound regeneration to the TIR1/AFB pathway and suggests that both inhibiting and activating auxin effects are mediated by this pathway. In this view, the reduced inhibitory effect in the *tir triple* mutant can be explained by the overall shift in sensitivity toward higher auxin concentration due to lack of some of the TIR1/AFB auxin receptors.

Auxin-Induced Cell Expansion in Wound Regeneration. The overproliferated, swollen roots observed after auxin treatment are the consequence of an increased number of restorative cell division and their consequent cell expansion. Given that auxin has a well-established role in growth both in roots and shoots (27–30), we analyzed changes in cell expansion during wound regeneration. We performed long-term imaging experiments in which we quantified the width of wound-adjacent cells as a proxy for cell expansion. After ablation, the size of the inner adjacent cells remained constant for a short "lag phase" (t_{lag}) of 0 to 4 h, followed by a phase of rapid expansion (t_{exp}), usually for 10 h, in which the cells grew continuously toward the wound and bulged toward the inner intact neighbor, suggesting increased turgor pressure. The expansion paused shortly during the time of division (t_{div}) and continued directly afterward (t_{exp2}) (Fig. 3 *A* and *B*; *SI Appendix*, Fig. S3 *A–C* and *F*; and Movie S6).

Auxin treatment reduced the expansion rate strongly in WT endodermis cells from 0.80 ± 0.3 μm/h to 0.42 ± 0.3 μm/h and slightly in cortex cells, from 0.68 ± 0.1 μm/h to 0.58 ± 0.2 μm/h (Fig. 3 *C* and *D* and *SI Appendix*, Figs. S3*D* and S4 *A–C*). The decreased expansion rates lead to a delay in cell size increase, which correlated with the decreased speed of restorative division induction (*SI Appendix*, Fig. S3*E*). In contrast, auxin treatment in the *tir triple* mutant strongly increased expansion in both the endodermis (1.0 ± 0.2 μm/h) and cortex (1.1 ± 0.3 μm/h) (Fig. 3 *C* and *D* and *SI Appendix*, Figs. S3*D* and S4 *B–D*), again correlating with higher rate of regeneration in these conditions. Collectively, these observations suggest that cell expansion is an important component of regeneration after wounding.

Notably, wound-adjacent cells in untreated WT plants exhibited stable cell expansion rates, which decreased only during mitosis. In contrast, cell expansion in auxin treated *tir triple* cells strongly fluctuated; phases of extremely high expansion (2 μm/h) were followed by a complete collapse (<0.5 μm/h) long before the onset of mitosis (*SI Appendix*, Fig. S4*E*). Steady cell expansion usually requires coordination of cell wall properties and turgor pressure, suggesting that this may be uncoupled in the case of *tir triple* on 1 μM NAA.

In summary, we observed that cell expansion correlates strongly with induction of regenerative divisions. Auxin has a similar dual effect on both cell expansion and regenerative division, presumably balancing turgor pressure and cell wall

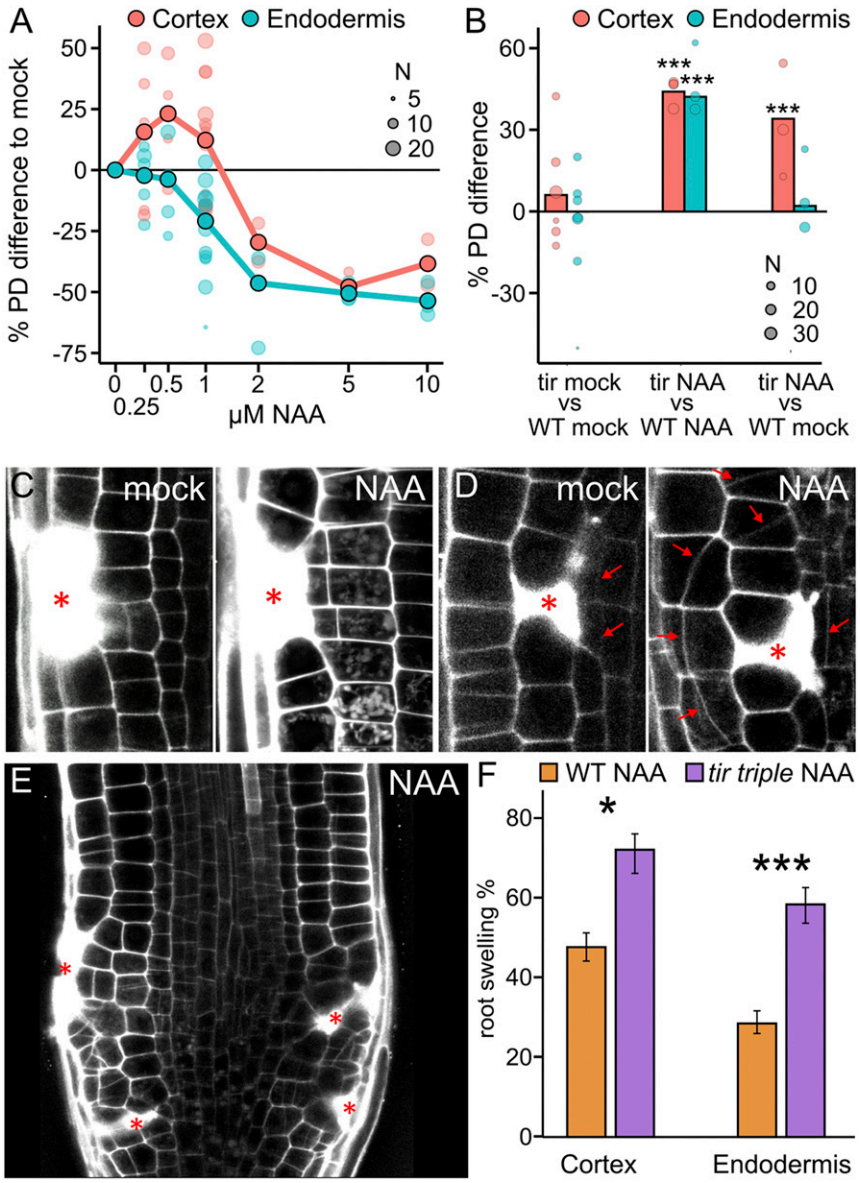

Fig. 2. Auxin effect on regeneration capacity. (*A*) Auxin increases division rates until 1 µM and decreases wound response at higher concentrations. Quantification of restorative periclinal division rates (in %) of endodermal (blue) and cortex (red) cells, after application of auxin in different concentrations (NAA; from 0 to 10 µM) compared with mock. Large dots represent weighted mean, and lighter dots represent individual experiments (area indicates sample size). (*B*) Auxin-treated *tir triple* mutant plants have higher division rates compared with WT plants. Quantification of relative restorative periclinal divisions rate (in %) of endodermal (blue) and cortex (red) cells, comparing the *tir triple* mutant with WT plants on mock, *tir triple* mutant with WT plants on 1 µM NAA treatment, or 1 µM NAA-treated *tir triple* with WT plants on mock. Data are represented as weighted mean difference (bar) and difference in individual experiments (dots; area indicates sample size). (*C* and *D*) Auxin expands zone of wound-responsive divisions. (*C*) Restorative cortex divisions on mock treatment (*Left*) or 1 µM NAA treatment (*Right*) after epidermal cell ablation (asterisk). (*D*) Restorative cell divisions in outer epidermis cells on mock treatment (*Left*) or 1 µM NAA treatment (*Right*) after cortex cell ablation (asterisk). Red arrows indicate new, oblique-periclinal cell plates. (*E*) Restorative cell divisions after cell ablations (marked with asterisk) in WT roots supplemented with 1 µM NAA. Note that the increment of restorative cell divisions in these conditions induces root swelling. (*F*) Quantification of root swelling (in %) after restorative cortex or endodermal cell division in 1 µM NAA-treated WT (orange bars) or *tir triple* (purple bars) background plants. Data are presented as ratios (bars), with error bars indicating upper and lower quartiles. Statistical significance was computed using the χ^2 test.

properties to regulate a steady growth toward the wound and permit accelerated periclinal divisions.

Auxin and Wounding in Activation of ERF115 Expression. ERF115 is a wound-responsive transcription factor and, so far, the prime candidate for mediating regeneration in plant roots. It is typically not expressed in the undisturbed root meristems but is highly up-regulated after removal of the root tip and is required for its restoration (5, 6, 10). After single-cell ablation, its expression is induced only in those one to three wound-adjacent endodermis or stele cells that later undergo wound-responsive divisions (Fig. 4*A*). In contrast, auxin (1 µM NAA) treatment, while having no effect in nonwounded roots, strongly induced *ERF115::GFP* expression around the wound (Fig. 4 *A* and *B*), spreading to all adjacent cells, including cortex cells and those above and below the ablation. Notably, ERF115 expression also expanded to cells nonadjacent to the wound, which normally do not undergo wound-responsive cell expansion and cell division.

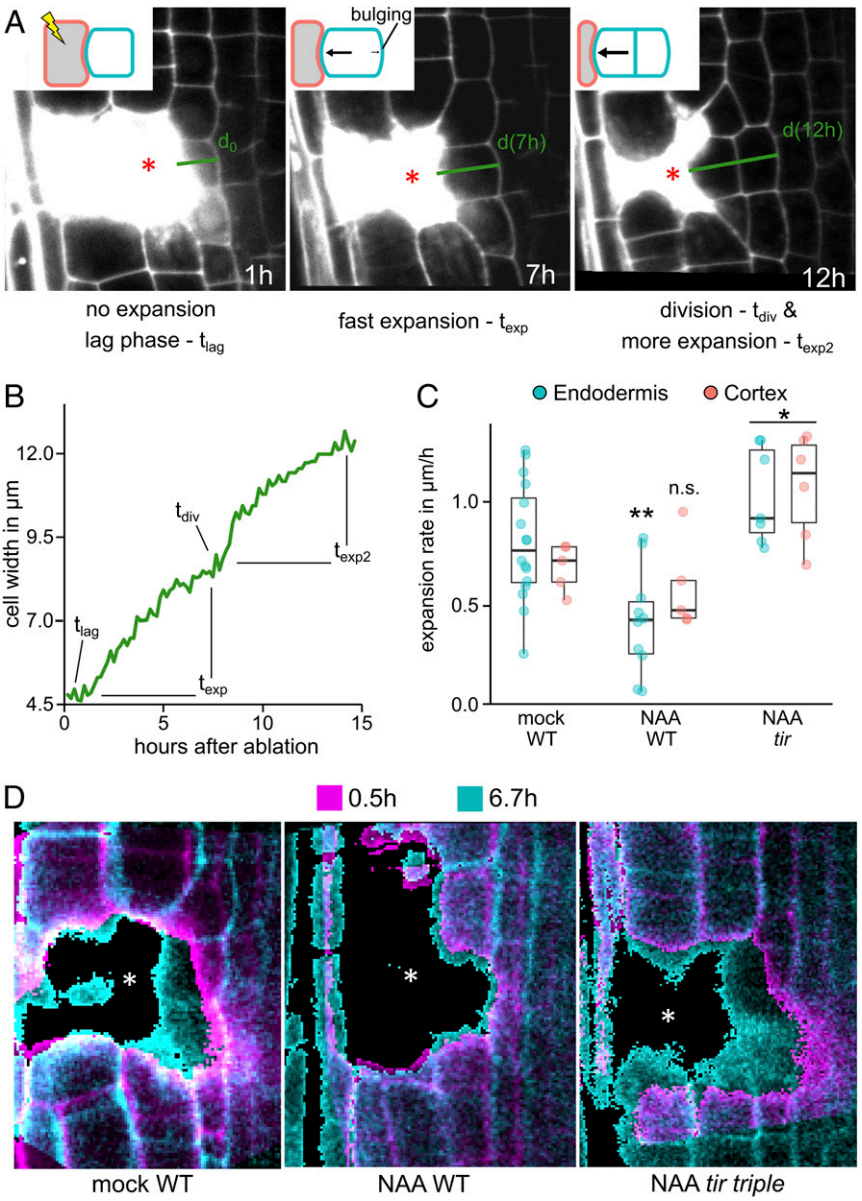

Fig. 3. Cell expansion during wound-responsive divisions. (*A* and *B*) Wound-adjacent cells undergoing restorative divisions are actively expanding toward the wound before the onset of division. (*A*) Cell expansion dynamics of an endodermal cell during wounding (cortex cell ablated; asterisk). Wound-induced cell expansion in endodermis at 1 h after cell ablation (*Left*), after 7 h (*Middle*), and after cell division at 12 h (*Right*). (*B*) Representation of the cell width (in µm) of a representative endodermis cell during the restorative cell division stages (in hours after ablation). t_{lag}, 0 to 1 h; t_{exp}, 1 to 7 h; t_{div}, 7 to 8 h; t_{exp2}, 8 to 15 h. (*C* and *D*) Premitotic cell expansion during auxin treatment is decreased in WT roots and increased in *tir triple* roots. (*C*) Representation of endodermal (blue) or cortex (red) cell expansion rate (µm/h) during restorative cell division in WT (mock- or 1 µM NAA-treated) or in *tir triple* roots on treatment with 1 µM NAA. Data are presented as premitotic expansion rates and dots indicating values from individual cells. Statistical significance was computed using Student's *t* test. (*D*) Overlay of wound-adjacent cell width at two different time points (0.5 h in magenta, and 6.7 h in cyan) after ablation in WT roots on mock treatment (*Left*), on 1 µM NAA treatment (*Middle*), and in 1 µM NAA-treated *tir triple* roots (*Right*). Asterisks denote ablated cells.

Overall, auxin induced an approximate eightfold increment of the *ERF115::GFP* expression after wounding (Fig. 4*C*).

We next evaluated *ERF115::GFP* expression using different auxin concentrations. We found that the minimum concentration of NAA required to enhance ERF115 was 100 nM NAA, which significantly increased the GFP intensity in the few cells undergoing restorative cell division. In contrast, the expression domain expanded only at higher concentrations such as 1 µM NAA (*SI Appendix*, Fig. S5*A*). To test the involvement of the canonical TIR1 pathway, we evaluated *ERF115::GFP* expression after wounding in *tir triple* root tips or in the *CCV-TIR1* background. Both genetic tools confirmed the involvement of TIR1/AFB signaling (*SI Appendix*, Fig. S5 *B* and *C*). Notably, *ERF115::GFP* expression was also absent in the untreated *tir triple* mutant (*SI Appendix*, Fig. S5*C*), suggesting involvement of TIR1/AFB auxin signaling in activation of ERF115 expression by endogenous auxin levels.

ERF115 expression also has been proposed to be regulated by other signals, such as methyl jasmonate (MeJA), H_2O_2, or brassinosteroids (6, 11, 12); nonetheless, unlike in the case of auxin, none of these other signals showed a pronounced effect on wound-responsive *ERF115::GFP* expression (*SI Appendix*, Fig.

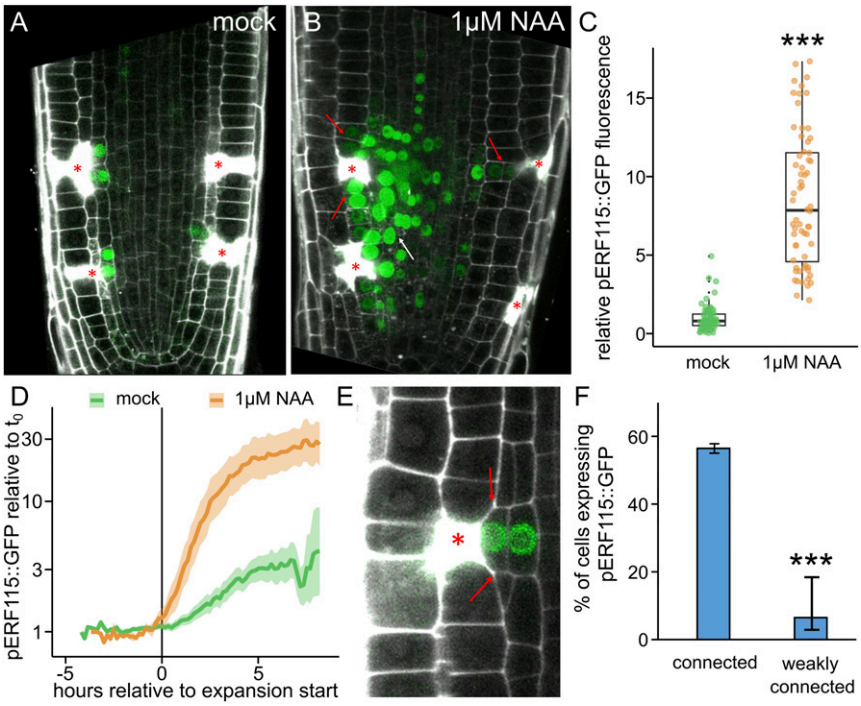

Fig. 4. ERF115 expression is connected to auxin and expansion. (*A–C*) Auxin application massively increases ERF115 expression around wounds. *ERF115::GFP* (green) expression on wound-adjacent cells on mock treatment (*A*) and on 1 μM NAA treatment (*B*). Asterisks denote ablated cells. Red arrows indicate *ERF115::GFP* expression expansion to wound-adjacent cortex cells, and the white arrow indicates *ERF115::GFP* expression expansion to non–wound-adjacent endodermis and stele cells. (*C*) Quantification of the relative *ERF115::GFP* fluorescence in wound-adjacent cells (normalized to the *ERF115::GFP* mean intensity on mock conditions), on mock treatment (green dots) or on μM NAA treatment. Data are represented as relative fluorescence intensity of individual cells. Statistical significance was computed using the two-sample Wilcoxon test. (*D–F*) *ERF115::GFP* expression correlates with premitotic expansion. (*D*) Quantification of *ERF115::GFP* relative gene expression (compared with t_0) of wound-adjacent cells before and after the expansion onset—t_{lag} (= 0 h)—on mock (green line) or on 1 μM NAA treatment (orange line). Lighter background represents SE. (*E*) Expression of *ERF115::GFP* in wound-adjacent cells after restorative cell division. Red arrows indicate junctions in which the cell is not fully connected to the wounded cell (asterisk). (*F*) Quantification of the percentage of cells expressing *ERF115::GFP*, grouped by grade of connection (connected or nonfully connected to the wound). Data are represented as ratios (bars) with error bars indicating upper and lower quartiles. Statistical significance was computed using the χ^2 test.

S6 *A–E*, *K*, and *L*). Ethylene, a wound-responsive hormone recently connected to the innate immune system in the *Arabidopsis* root after wounding and single-cell ablation (7, 31), did not influence ERF115 expression (9) (*SI Appendix*, Fig. S6 *F–H*) and decreased the amount of restorative divisions in the meristem only slightly (*SI Appendix*, Fig. S6*I*). Application of other hormones related with cell wound response, including salicylic acid (SA) and abscisic acid (ABA), also did not change the *ERF115::GFP* expression after wounding (*SI Appendix*, Fig. S6 *J* and *M*). These results suggest that auxin is rather a specific signal regulating *ERF115::GFP* expression after wounding, although not the primary trigger for its activation.

Auxin-Regulated Cell Expansion and Activation of ERF115 Expression. Since auxin regulates both cell expansion and ERF115 expression after wounding, we performed long-term, live observations to investigate possible correlation between these processes. Indeed, even in absence of auxin treatment, we found that cells with higher expansion rates also had increased *ERF115::GFP* signals (*SI Appendix*, Fig. S7*E*). In addition, we observed that *ERF115::GFP* expression was absent from those cells that were only weakly connected to the wound and thus did not trigger cell expansion (Fig. 4 *E* and *F*).

Given this strong spatial connection between ERF115 expression and wound-responsive expansion, we investigated their time dynamics to gain insight into their interdependency. ERF115 expression was detectable only after the onset of expansion (Fig. 4*D*), ruling out ERF115 as a major activator of wound-responsive expansion. However, after treatment with auxin, ERF115 expression coincided with or preceded the onset of expansion (Fig. 4*D*). Considering the temporal dynamics of upstream transcriptional regulation and GFP maturation, this also ruled out the possibility that ERF115 expression is a direct consequence of cell expansion.

In conclusion, wound-responsive activation of ERF115 expression and cell expansion were strongly correlated spatially and temporary, but did not directly depend on each other, suggesting an as-yet unknown wound-induced upstream signal activating both.

Tissue Integrity and Turgor in Wound Regeneration. Given the here identified importance of cell expansion for both the regenerative divisions and ERF115 expression, we hypothesized that rapid, nongenetic factors, such as collapse of injured cells and changes in turgor or cell wall tension, may be important early cues for inducing regeneration processes. Therefore, we investigated more closely the immediate responses of the targeted cell and its surrounding neighbors during ablation-induced injury. Following ablation, the cellular content of the killed cells was released to the environment, resulting in a pressure drop, which was visible as a strong bulging of the neighboring cells toward the wound (*SI Appendix*, Fig. S7*A* and Movie S7). In those neighboring cells, we observed a rapid displacement of nuclei (*SI Appendix*, Fig. S7*C*) and a slow reduction of the initial bulging (*SI Appendix*, Fig. S7*B* and Movie S7), suggesting a loss of cell volume in the neighboring cells. Over a longer time (>60 s), pressure built up again

in the neighboring cells, and they again bulged toward the wound (*SI Appendix*, Fig. S7*A*). Notably, the release of cellular content and rapid pressure changes as quantified by instant nucleus displacement were absent from roots during treatment with hyperosmotic, 0.5 M mannitol (*SI Appendix*, Fig. S7 *D* and *G*). This suggests that the collapse of killed cells causes a strong turgor pressure shock in the neighboring cells, influencing cell expansion and ERF115 expression.

In support of this idea, treatment with mannitol strongly decreased wound-induced cell expansion and wound-triggered periclinal divisions (Fig. 5 *A* and *B*). Notably, the normally occurring, anticlinal (nonrestorative, proliferative) divisions were still ongoing under these hyperosmotic conditions (*SI Appendix*, Fig. S7*F*). In addition, the bulging of cell walls toward the inner neighbors, indicative of changes in turgor pressure, was significantly reduced during mannitol treatment (*SI Appendix*, Fig. S7 *G* and *H*). This implies that changes in turgor are specifically required for regenerative, but not proliferative, divisions.

We next evaluated the effect of hyperosmotic treatment on *ERF115::GFP* expression by applying different concentrations of mannitol to locally injured roots. In contrast to cell expansion, we observed that at mannitol concentrations of 0.23 M and 0.3 M, the ERF115 expression was only slightly reduced after wounding in both mock and auxin (1 μM NAA) treatment. Of note, only hyperosmotic treatment with 0.5 M mannitol inhibited *ERF115::GFP* expression in the wounded root tips (Fig. 5 *C* and *D*), suggesting that cell collapse after wounding, which is absent at treatment with 0.5 M mannitol (see above), is crucial for triggering ERF115 expression.

This finding prompted us to test the importance of the collapse of the ablated cells for cell expansion, ERF115 expression, and regeneration. To this end, we modified the UV ablation technique by reducing the laser power to 50%. We regularly managed to harm the cell envelope between two cells rather than the whole cells (Fig. 5 *E* and *F*). These harmed cells usually did not induce ERF115 expression (Fig. 5*G*). However, in rare cases, these cells specifically triggered ERF115 induction, which was strongly enhanced by auxin treatment (Fig. 5*G* and *SI Appendix*, Fig. S7*I*). They also induced periclinal cell divisions, accompanied by minor cell expansion on rare occasions (*SI Appendix*, Fig. S7*J*), suggesting minor wound signaling without cell collapse

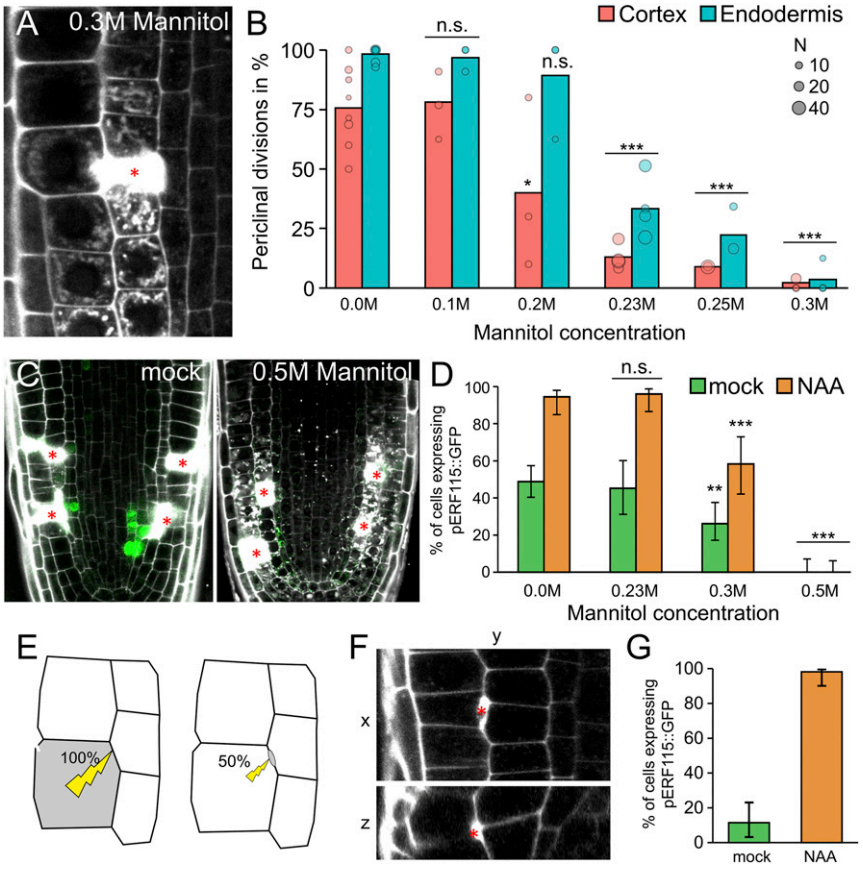

Fig. 5. ERF115 expression correlates with expansion induction. (*A* and *B*) Hyperosmotic treatment inhibits restorative periclinal divisions. (*A*) Cortex cell ablation at 12 h after ablation during 0.3 M mannitol treatment. (*B*) Quantification of restorative periclinal division rates (in %) of endodermal (blue) and cortex (red) cells, after treatment with different concentrations of mannitol (from 0 to 0.3 M). Bars represent weighted means, and dots represent individual experiments (area indicates sample size). Statistical significance was computed from conditional logistic regression. (*C* and *D*) Hyperosmotic treatment reduces ERF115 induction. (*C*) *ERF115::GFP* (green) expression on root tips after cell ablation (wounding) in mock conditions (*Left*) or in media supplemented with 0.5 M mannitol (*Right*). (*D*) Quantification of wound-adjacent cells expressing *ERF115::GFP* on mock treatment (green bars) or on auxin treatment (NAA; orange bars) in media supplemented with differing mannitol concentrations (from 0 to 0.3 M). Data are presented as ratios (bars), and error bars indicate upper and lower quartiles. Statistical significance was computed using the χ^2 test. (*E*–*G*) Harming only the cell envelope does not trigger ERF115 induction. (*E*) Schematic representation of cell wounding after application of 100% or 50% laser power during laser cell ablation. (*F*) Harmed cell region after using 50% laser power presented as vertical section (XY; *Upper*) and horizontal projection (ZY; *Lower*). Cell harming is stained by a strictly confined PI accumulation (in white, red asterisk). (*G*) Quantification of the percentage of wound-adjacent cells expressing *ERF115::GFP* after using 50% laser power in root tips on mock treatment or on 1 μM NAA treatment. Data are presented as ratios (bars), and error bars indicate upper and lower quartiles.

through cell wall integrity sensing or minor pressure changes after cell envelope harm.

This suggests that cellular collapse after wounding is crucial for ERF115 expression and wound-responsive cell expansion. Furthermore, turgor pressure stress after ablation is a component of the wound response and, together with the local increase in auxin signaling, might influence fast and efficient regeneration.

Discussion

In this work, we addressed the question of how plants can effectively regulate the coordination of wound responses on a cellular level to mediate tissue regeneration. We found that local induction of auxin signaling in concert with wound-induced nongenetic mechanisms, such as local expansion of cells in the wound vicinity, play major roles in this process. In summary, our data show how strictly localized auxin signaling coordinates the wound responses by regulating cell division rates, cell expansion rates, and transduction of the wound signal through activation of the ERF115 transcription factor (*SI Appendix*, Fig. S8).

Our data also show that turgor-driven swelling of the wound-adjacent cells is crucial for the initiation of restorative divisions and subsequent regeneration. This shows interesting similarities/parallels to the initiation of lateral root primordia, where pericycle cells swell before induction of asymmetric divisions (32). This process requires that the overlying endodermis cells shrink or collapse, which can be imitated by local ablation of endodermis cells in the elongation zone (33). The capacity to divide after ablation in the pericycle is independent of auxin signaling; however, local auxin signaling is essential in this context for the induction of a formative and asymmetric first division, leading to the proper formation of lateral root primordia (33, 34). We have observed a similar phenomenon; a local auxin increase in cells adjacent to the wound regulates both their expansion and division during regeneration. An accumulation of auxin could have many sources, for example, release from conjugates or a production from less well known alternative biosynthetic pathways, altered auxin importer activity, or a general release from the plasmodesmata-associated ER as consequence of the disrupted connection to the ablated neighbor. Since such processes are difficult to study, the origin has remained elusive; however, daughters of wound-adjacent cells also exhibit increased auxin signaling activity, implying an active process working throughout the duration of regeneration.

Auxin has a well-established role in expansion on a cellular level, through cell wall remodeling (35), and on a tissue level, through hydraulic pressure regulation (36). The biphasic mode of auxin in cell wall remodeling (27) shares similarities with our observed dual auxin effect of promoting and inhibiting cell expansion and restorative divisions, thus suggesting a negative feedback loop in which prolonged auxin signaling would inhibit wound-responsive division and expansion at the end of the regeneration process. The overproliferation of cells and the tissue swelling after wounding is similar to defects in lateral root primordia initiation during disturbed auxin signaling (37), suggesting that accurate auxin signaling is crucial for the regulation of wound-responsive cell expansion and divisions.

The turgor pressure—or osmotic—stress in the adjacent cells following wounding might be a key component in the wound signaling mechanism, as has been suggested in other tissues (38, 39). Recently, a similar, locally restricted induction of wound responses in the root—the activation of immune signaling—has been proposed to be caused by local pressure changes (31). Notably, the wound-responsive expression of ERF115 is also inducible by osmotic stress (40), and a direct target of ERF115 includes one member of the expansin family (9); cell wall remodeling proteins expressed during osmotic stress to maintain steady growth even during reduced turgor pressure (41). This suggests that ERF115 is a key component of a hydraulic/osmotic stress response after wounding and might be involved in integrating auxin signaling and pressure stress to define the zone of wound response and to both induce and spatially restrict regeneration processes.

Further investigation of the induction of ERF115 expression as a marker for restorative patterning and involvement of other components suggested in wounding responses in the root could help reveal upstream regulators of such local yet distinctive regeneration processes of inducing cell expansion and targeted, restorative cell divisions.

Methods

Plant Material. *Arabidopsis thaliana* (L.) Heynh (accession Columbia-0) was used in this work (WT). The following transgenic *A. thaliana* lines and mutant lines were described previously: *RPS5A::mDII-ntdTomato-RPS5A::DII-n3Venus* (R2D2) (18), *HTR5::NLS-GFP* (42), *tir1-1 afb2-1 afb3-1* (*tir triple*) (24), *CCV-TIR1 tir1-1 afb2-1* (26), *ERF115::NLS-GFP-GUS* (*ERF115::GFP*) (10), *ERF115::NLS-GFP–GUS coi1-2* (6), and *35S::MAP4-GFP* (43). *ERF115::NLS-GFP-GUS* was introduced into the *tir1-1 afb2-1 afb3-1* and *CCV-TIR1* backgrounds by genetic crossing. *tir1-1 afb2-1 afb3-1* seedlings were identified by PCR-cased genotyping (24) in F2 and F3 generations *ERF115::NLS-GFP-GUS*, and *CCV-TIR1* carrying plants were identified in F2, F3, and F4 generations by kanamycin and basta resistance, respectively.

Growth Conditions. Seeds of *A. thaliana* were sown on Murashige & Skoog (M&S) medium (Duchefa Biochemie) with 1% sucrose and 1% agar, stratified for 1 to 2 d, and grown for 3 to 5 d at 21 °C on a 16-h light/8-h dark cycle.

Pharmacologic Treatments. Seedlings were transferred on solid M&S medium containing the indicated chemicals: propidium iodide (PI; 10 μM, Sigma-Aldrich or Thermo Fisher Scientific), NAA (Duchefa Biochemie; final concentration if not indicated otherwise, 1 μM), NPA (final concentration 10 μM), yucasin (Wako Chemicals; final concentration 100 μM), L-kynurenine (Sigma-Aldrich, final concentration 10 or 50 μM, as indicated), CVX-IAA (Tokyo Chemical Industry, final concentration 250 nM), MeJA (Sigma-Aldrich, final concentration 50 μM), hydrogen peroxide (Sigma-Aldrich, final concentration 200 μM), (±)ABA (Sigma-Aldrich, final concentration 25 μM), epibrassinolide (Sigma-Aldrich, final concentration 1 μM), brassinazole (Sigma-Aldrich, final concentration 1 μM), SA (Sigma-Aldrich, final concentration 40 μM), and mannitol (Sigma-Aldrich, final concentration 0.1 to 0.5 M, as indicated).

Sample Preparation. Seedlings were placed on chambered cover glass (Nunc Lab-Tek; Thermo Fisher Scientific) as described previously (44). With the chamber, a block of solid M&S medium was cut out, and PI solution was added. Once the liquid soaked in, 10 to 15 seedlings were transferred to the agar, and the block was inserted into the chamber.

Confocal Imaging and Image Processing. Confocal imaging was performed with Zeiss LSM700/800 inverted microscopes using a 20× or 40× objective or a spinning-disk imaging system. Detection of fluorescence signals was done for GFP (excitation wavelength, 488 nm; emission wavelength, 507 nm), YFP (excitation wavelength, 514 nm; emission wavelength, 527 nm) and PI (excitation wavelength, 536 nm; emission wavelength, 617 nm). For fixed time point measurements, samples were observed at 12 h after ablation or at indicated time points. Images were analyzed using ImageJ (http://rsb.info.nih.gov/ij) and Zeiss Zen 2.3 "Black" or "Blue" software. Where necessary, images were processed by adjusting contrast and lightness.

Spinning-Disk Imaging. For the observation of immediate effects during/after ablation, an Andor spinning disk microscope (CSU X-1, iXon 897 camera [back-thinned EMCCD], FRAPPA unit, and motorized piezo stage) with a 63× water immersion objective was used. Videos were acquired with one focal plane every 0.2 s, for 1 to 10 min. All images in a single experiment were captured with the same settings.

Vertical Stage Microscopy, Root Tracking, and Image Processing. Vertical stage microscopy for long-term tracking of root meristems was performed as described previously (5, 19). Roots were imaged with a vertically positioned Zeiss LSM700 or LSM800 inverted confocal microscope and Zeiss Zen 2.3 "Black" or "Blue" software, respectively, with a 20× objective and detection of PI, GFP (see above), and transmitted light. Z-stacks of 30 to 42 μm were set accordingly to image each cell at least once. For root tracking, the TipTracker MATLAB script (Zen Black) or the TipTracker internal macro (Zen Blue) were

used; interval duration was set between 600 s (10 min) and 720 s (12 min). The resulting images were concatenated and analyzed using ImageJ. For registration, ImageJ macros "correct 3D drift," "StackReg," and "MultiStackReg" were used. Kymographs were generated using the "Reslice" tool and restacked in case of nonregistered videos.

UV Laser Ablation Setup. UV laser ablation was performed as described previously (5, 33), based on a previously published layout (45). For the cell envelope harming, we used 50% of the laser power needed for the elimination of a full cell. The laser was applied in the upper corner of the outer neighboring cell of the cell of interest (Fig. 5*C*).

Quantification and Statistical Significance. Asterisks illustrate the *P* value: $***P < 0.001$; $**P < 0.01$; $*P < 0.05$.

Periclinal Divisions. For counting the (absolute) amount of periclinal divisions after ablation, the number of ablations with and without periclinal divisions (division plane parallel or oblique to the growth axis) in any of the adjacent cells (if nothing else indicated, only inner cells) were recorded, and the ratio of positive events to all events was calculated. For the differences, the ratios for each sample experiments were subtracted from the respective control experiment (untreated WT). The mean of these differences from multiple experiments was weighted based on the sample size.

As described previously (5), the binary data were analyzed using conditional logistic regression (46, 47), pairing the data within individual experiments. The statistical significance was computed using the clogit function from the R package "survival".

Fluorescence Intensity in Time Series Experiments. The signal intensity of each observed nucleus from multistack three-dimensional (3D) videos in the green (or red, for mDII-ntdTomato) channel was quantified using ImageJ and recorded for each available time frame. Similarly, data from reference nuclei (neighboring, nonadjacent cells) was recorded, and the ratio of sample to reference value was calculated for each single time point. For *ERF115::GFP*, the ratio of each time frame to the first time frame was calculated.

Statistical significance was calculated on the ratios using a one-sample Wilcoxon test (based on the nonnormal distribution of the data) using wilcox.test() in R with $\mu = 1$ (reference cell).

Cell Expansion. Cell expansion was approximated by the cell width, which was quantified as the distance between the midpoint of the cell wall segment touching the ablation site and the midpoint of the opposite cell wall at each time point using ImageJ. Expansion rates were calculated between the onset of expansion (end of lag phase) and the initiation of cell division (nuclear envelope breakdown). Statistical significance between samples was calculated with Student's *t* test using t.test() in R. For calculating the point of expansion collapse (*SI Appendix*, Fig. S4*E*), expansion rates at each time point were calculated from cell width expansion throughout the previous five time frames (50 min). The point of expansion collapse was determined as the first time point at which the expansion rate dropped below 1 μm/h.

Cell Wall Bulging. The distance between the midpoint of a straight line connecting the two cell corners facing the inner adjacent cell and the midpoint of the cell wall facing the inner adjacent neighbor was calculated as inner cell wall bulging. The values obtained from wound-adjacent cells were subtracted from the closest, nonadjacent cells of the same cell type (usually the direct neighbor).

The statistical significance was calculated using the two-sample Wilcoxon test between the mock and mannitol treatment values with wilcox.test() in R.

Nucleus Displacement. The distance of nucleus movement/displacement directly after ablation was measured until maximum 5 s after ablation from videos obtained from a spinning disk imaging system (1 frame per 0.2 s). The statistical significance was calculated using a two-sample Wilcoxon test between the mock and the Mannitol treatment values with wilcox.test() in R.

Fluorescence Intensity in Fixed Time Point Experiments. For quantitative measurements, the signal intensity of all wound adjacent (inner) cells within one focal plane was measured using ImageJ in the green channel. Each obtained value from one experiment/repetition was divided by the mean fluorescence intensity in the reference sample (untreated WT) to obtain (comparable) relative fluorescence intensities.

The statistical significance was calculated using the two-sample Wilcoxon test between the reference and the sample values with wilcox.test() in R.

For qualitative data, the numbers of cells with and without visible GFP accumulation in the nucleus were counted, and the ratio of positive to all observed events was computed. For the error bars, the borders of the upper and lower quartiles were calculated assuming a beta distribution of the binary values with qbeta() in R.

The statistical significance was computed with the χ^2 test for binary data using the chisq.test() function in R.

Data Availability. The R code for computing statistical significance for binary data using a conditional logistic regression is provided in *SI Appendix*, Code S1. Raw data in the form of microscopy images and compiled videos can be accessed at https://www.ebi.ac.uk/biostudies/BioImages/studies/S-BIAD23 under accession no. S-BIAD23.

ACKNOWLEDGMENTS. We thank Ben Scheres, Dolf Weijers, Keiko Torii, Lieven De Veylder, Mark Estelle, and Moritz Nowak for sharing published material. We thank the staff at the Bioimaging and Life Science Facilities at Institute of Science and Technology Austria for their invaluable assistance. The research leading to these results received funding from the European Research Council (ERC) under the European Union's Seventh Framework Programme (FP7/2007-2013)/ERC grant agreement 742985 and from the Austrian Science Fund under stand-alone grant P29988.

1. C. van den Berg, V. Willemsen, W. Hage, P. Weisbeek, B. Scheres, Cell fate in the Arabidopsis root meristem determined by directional signalling. *Nature* **378**, 62–65 (1995).
2. F. Berger, J. Haseloff, J. Schiefelbein, L. Dolan, Positional information in root epidermis is defined during embryogenesis and acts in domains with strict boundaries. *Curr. Biol.* **8**, 421–430 (1998).
3. M. Ikeuchi *et al*., Molecular mechanisms of plant regeneration. *Annu. Rev. Plant Biol.* **70**, 377–406 (2019).
4. L. Hoermayer, J. Friml, Targeted cell ablation-based insights into wound healing and restorative patterning. *Curr. Opin. Plant Biol.* **52**, 124–130 (2019).
5. P. Marhava *et al*., Re-activation of stem cell pathways for pattern restoration in plant wound healing. *Cell* **177**, 957–969.e13 (2019).
6. W. Zhou *et al*., A jasmonate signaling network activates root stem cells and promotes regeneration. *Cell* **177**, 942–956.e14 (2019).
7. P. Marhavý *et al*., Single-cell damage elicits regional, nematode-restricting ethylene responses in roots. *EMBO J.* **38**, e100972 (2019).
8. T. Hander *et al*., Damage on plants activates $Ca2^+$-dependent metacaspases for release of immunomodulatory peptides. *Science* **363**, eaar7486 (2019).
9. J. Heyman *et al*., ERF115 controls root quiescent center cell division and stem cell replenishment. *Science* **342**, 860–863 (2013).
10. J. Heyman *et al*., The heterodimeric transcription factor complex ERF115-PAT1 grants regeneration competence. *Nat. Plants* **2**, 16165 (2016).
11. H.-S. Lee *et al*., Brassinazole-resistant 1 (BZR1)-dependent brassinosteroid signalling pathway leads to ectopic activation of quiescent cell division and suppresses columella stem cell differentiation. *J. Exp. Bot.* **66**, 4835–4849 (2015).
12. X. Kong *et al*., PHB3 maintains root stem cell niche identity through ROS-responsive AP2/ERF transcription factors in Arabidopsis. *Cell Rep.* **22**, 1350–1363 (2018).
13. D. Xu *et al*., YUCCA9-mediated auxin biosynthesis and polar auxin transport synergistically regulate regeneration of root systems following root cutting. *Plant Cell Physiol.* **58**, 1710–1723 (2017).
14. I. Efroni *et al*., Root regeneration triggers an embryo-like sequence guided by hormonal interactions. *Cell* **165**, 1721–1733 (2016).
15. Z. Ding, J. Friml, Auxin regulates distal stem cell differentiation in Arabidopsis roots. *Proc. Natl. Acad. Sci. U.S.A.* **107**, 12046–12051 (2010).
16. J. Xu *et al*., A molecular framework for plant regeneration. *Science* **311**, 385–388 (2006).
17. S. Yoshida *et al*., Genetic control of plant development by overriding a geometric division rule. *Dev. Cell* **29**, 75–87 (2014).
18. C. Y. Liao *et al*., Reporters for sensitive and quantitative measurement of auxin response. *Nat. Methods* **12**, 207–210, 2, 210 (2015).
19. D. von Wangenheim *et al*., Live tracking of moving samples in confocal microscopy for vertically grown roots. *eLife* **6**, e26792 (2017).
20. M. Glanc, M. Fendrych, J. Friml, Mechanistic framework for cell-intrinsic re-establishment of PIN2 polarity after cell division. *Nat. Plants* **4**, 1082–1088 (2018).
21. T. Nishimura *et al*., Yucasin is a potent inhibitor of YUCCA, a key enzyme in auxin biosynthesis. *Plant J.* **77**, 352–366 (2014).
22. W. He *et al*., A small-molecule screen identifies L-kynurenine as a competitive inhibitor of TAA1/TAR activity in ethylene-directed auxin biosynthesis and root growth in Arabidopsis. *Plant Cell* **23**, 3944–3960 (2011).
23. J. Zhu *et al*., TWISTED DWARF1 mediates the action of auxin transport inhibitors on actin cytoskeleton dynamics. *Plant Cell* **28**, 930–948 (2016).
24. N. Dharmasiri *et al*., Plant development is regulated by a family of auxin receptor F box proteins. *Dev. Cell* **9**, 109–119 (2005).

25. M. J. Prigge, N. Kadakia, K. Greenham, M. Estelle, Members of the Arabidopsis auxin receptor gene family are essential early in embryogenesis and have broadly overlapping functions. bioRxiv. 10.1101/529248 (2019).
26. N. Uchida *et al*., Chemical hijacking of auxin signaling with an engineered auxin-TIR1 pair. *Nat. Chem. Biol.* **14**, 299–305 (2018).
27. E. Barbez, K. Dünser, A. Gaidora, T. Lendl, W. Busch, Auxin steers root cell expansion via apoplastic pH regulation in Arabidopsis thaliana. *Proc. Natl. Acad. Sci. U.S.A.* **114**, E4884–E4893 (2017).
28. M. Fendrych *et al*., Rapid and reversible root growth inhibition by TIR1 auxin signalling. *Nat. Plants* **4**, 453–459 (2018).
29. M. Fendrych, J. Leung, J. Friml, TIR1/AFB-Aux/IAA auxin perception mediates rapid cell wall acidification and growth of Arabidopsis hypocotyls. *eLife* **5**, e19048 (2016).
30. H. Ren, W. M. Gray, SAUR proteins as effectors of hormonal and environmental signals in plant growth. *Mol. Plant* **8**, 1153–1164 (2015).
31. F. Zhou *et al*., Co-incidence of damage and microbial patterns controls localized immune responses in roots. *Cell* **180**, 440–453.e18 (2020).
32. J. E. M. Vermeer *et al*., A spatial accommodation by neighboring cells is required for organ initiation in Arabidopsis. *Science* **343**, 178–183 (2014).
33. P. Marhavý *et al*., Targeted cell elimination reveals an auxin-guided biphasic mode of lateral root initiation. *Genes Dev.* **30**, 471–483 (2016).
34. P. Marhavý *et al*., Auxin reflux between the endodermis and pericycle promotes lateral root initiation. *EMBO J.* **32**, 149–158 (2013).
35. M. Majda, S. Robert, The role of auxin in cell wall expansion. *Int. J. Mol. Sci.* **19**, 951 (2018).
36. B. Péret *et al*., Auxin regulates aquaporin function to facilitate lateral root emergence. *Nat. Cell Biol.* **14**, 991–998 (2012).
37. J. G. Dubrovsky *et al*., Auxin minimum defines a developmental window for lateral root initiation. *New Phytol.* **191**, 970–983 (2011).
38. P. Reymond, H. Weber, M. Damond, E. E. Farmer, Differential gene expression in response to mechanical wounding and insect feeding in Arabidopsis. *Plant Cell* **12**, 707–720 (2000).
39. M. Denekamp, S. C. Smeekens, Integration of wounding and osmotic stress signals determines the expression of the AtMYB102 transcription factor gene. *Plant Physiol.* **132**, 1415–1423 (2003).
40. P. Krishnamurthy *et al*., Transcriptomics analysis of salt stress tolerance in the roots of the mangrove Avicennia officinalis. *Sci. Rep.* **7**, 10031 (2017).
41. R. Tenhaken, Cell wall remodeling under abiotic stress. *Front Plant Sci* **5**, 771 (2015).
42. M. Ingouff *et al*., Live-cell analysis of DNA methylation during sexual reproduction in Arabidopsis reveals context and sex-specific dynamics controlled by noncanonical RdDM. *Genes Dev.* **31**, 72–83 (2017).
43. J. Marc *et al*., A GFP-MAP4 reporter gene for visualizing cortical microtubule rearrangements in living epidermal cells. *Plant Cell* **10**, 1927–1940 (1998).
44. P. Marhavý, E. Benková, Real-time analysis of lateral root organogenesis in Arabidopsis. *Bio Protoc.* **5**, e1446 (2015).
45. J. Colombelli, S. W. Grill, E. H. K. Stelzer, Ultraviolet diffraction limited nanosurgery of live biological tissues. *Rev. Sci. Instrum.* **75**, 472–478 (2004).
46. M. J. Campbell, *Statistics at Square Two: Understanding Modern Statistical Applications in Medicine*, (Wiley, 2013).
47. D. G. Kleinbaum, M. Klein, *Logistic Regression: A Self-Learning Text*, (Springer, ed. 3, 2010).